ACS APPLIED MATERIALS & INTERFACES

Research Article

www.acsami.org

Uniaxially Aligned Nanofibrous Cylinders by Electrospinning

Soumen Jana, Ashleigh Cooper, Fumio Ohuchi, and Miqin Zhang*

Department of Materials Science & Engineering, University of Washington, Seattle, Washington 98195, United States

ABSTRACT: Aligned nanofibers have drawn increasing interest for applications in biomedical engineering, electronics, and energy storage systems owing to the unique physicochemical properties provided by their anisotropy and high surface-to-volume ratio. Nevertheless, direct fabrication or assembly of aligned nanofibers into a 3-dimensional standalone construct with practically applicable dimensions presents an enormous challenge. We report a facile method to fabricate aligned nanofibrous cylinders, a widely used geometric form, by electrospinning aligned nanofibers across the gap between a pair of pin electrodes placed apart uniaxially. With this approach, cylindrical nanofibrous constructs of several millimeters in diameter and several centimeters in length can be readily produced. The versatility of the approach was demonstrated with several commonly used polymeric and ceramic materials, including polycaprolactone (PCL), chitosan/PCL, polyvinylidene fluoride, and titania. For a model application in tissue engineering, skeletal muscle cells were cultured on nanofibrous cylinders, which effectively produced highly aligned and densely populated myotubes along the nanofiber orientation, favorable for muscle tissue regeneration. With high structural integrity and stability, these can be directly integrated into devices or implanted in vivo as a standalone construct without the support of a substrate, thus increasing the portability, efficiency, and applicability of aligned nanofibers.

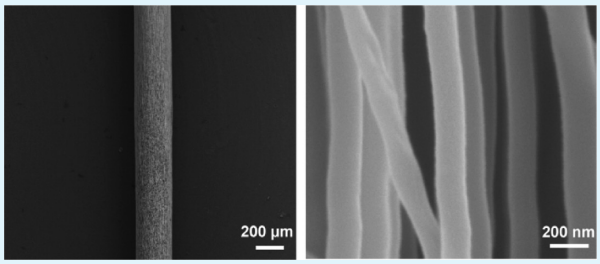

KEYWORDS: *nanofiber, aligned, cylindrical rod, electrospinning, tissue engineering*

INTRODUCTION

Aligned nanofibrous materials have drawn considerable attention in the past decade for applications in tissue engineering,[1−4] drug delivery,[5,6] electronics,[7−9] and energy storage systems[10−13] because of the tremendous benefits provided by their anisotropic biological, mechanical, electrical, or optical properties. For example, in skeletal muscle tissue engineering, cells demonstrated increased proliferation and up-regulation of differentiation-specific gene expression on aligned nanofibrous scaffolds compared to randomly oriented nanofibers.[14] In nerve regeneration, aligned nanofibers appeared to enhance Schwann cell maturation manifested by up-regulation of myelin-related gene expression.[15] In electronics, a membrane composed of aligned sulfonated polyimide nanofibers exhibited a proton conductivity in the axial direction 3 and 10 times greater than in the perpendicular direction and in a membrane of nonfibrous structure, respectively.[12] Electrodes made of vertically grown, 2-μm long aligned carbon nanofibers demonstrated an increase of ∼20 times in interfacial capacitance compared to planar electrodes due to an increased surface area.[16] In these applications, nanofibers or nanofibrous membranes are deposited or placed on a substrate to retain their structure integrity, which can be thought of as a two-dimensional configuration. Clearly, the ability to directly fabricate or assemble standalone nanofibrous constructs with desired three-dimensional (3D) geometry would vastly broaden the applicability and enhance the performance efficacy of these nanomaterials.

Compared to other methods (e.g., phase separation, self-assembly, template-directed synthesis), electrospinning is a relatively simple and versatile approach for production of polymer-based nanofibrous structures.[17−19] Aligned nanofibers can be electrospun by using specially designed collectors such as a fast rotating mandrel or a pair of parallel electrodes.[18] In the fast rotating collector configuration, polymer fibers are deposited on the surface of the mandrel and oriented perpendicular to the rotating axis. In the parallel-electrode configuration, charged fibers are aligned across an insulating gap between the two electrodes. Despite the ability to produce aligned fibers, only 2D fibrous mats or membranes with limited size and thickness could be produced from these systems. These 2D constructs cannot be normally used directly in devices or applications and a substrate support to maintain their structural integrity is often required.[20] 3D tubular nanofibrous constructs have been made by manually rolling a nanofibrous membrane on a metal rod with multiple layers followed by the removal of the metal rod.[21,22] The method has difficulties in maintaining its morphology intact, a uniform thickness, and close interactions of fibers between layers.

Here, we report a facile method to fabricate standalone highly aligned 3D nanofibrous cylinders, a geometric form commonly used in biomedical, electronic, and other engineering applications. The nanofibrous cylinders were produced by electrospinning across the gap between two uniaxially aligned pin electrodes in a layer-by-layer fashion. In our system configuration, the geometric dimensions of the produced

Received: June 25, 2012
Accepted: September 4, 2012
Published: September 4, 2012

   dx.doi.org/10.1021/am301803b | ACS Appl. Mater. Interfaces 2012, 4, 4817−4824

cylinder can be varied by the width of the electrode gap and the duration of electrospinning, which can be up to several centimeters in length and several millimeters in diameter.

The versatility of this technique was demonstrated with several materials, including three polymers (polycaprolactone (PCL), polyvinylidene fluoride (PVDF), and chitosan/PCL), and a metal oxide (titania). These materials were chosen due to their wide-range applicability. PCL and chitosan[23] are relevant to diverse applications in tissue engineering; PVDF[24] is commonly used in sensing applications, and titania (TiO_2) is widely used for applications in gas sensing, solar cells, photocatalysis, and environmental cleaning.[25] As a first model application of 3D aligned nanofibrous structure, we demonstrate the guided growth of myotubes on an aligned chitosan/PCL fibrous cylinder for skeletal muscle tissue engineering.

EXPERIMENTAL SECTION

Electrospinning Solutions. A 12 wt % PCL (MW 90,000 Da, Aldrich, St. Louis, MO) solution was prepared in 2,2,2-trifluoroethanol (TFE, Aldrich) by stirring overnight. To prepare the chitosan solution, practical grade chitosan (MW 100 000−300 000 Da, Polysciences, Warrington, PA) was dissolved in trifluoroacetic acid (TFA, Aldrich) at 7 wt % by refluxing at 80 °C for 3 h. Twelve wt % PCL and 7 wt % chitosan solutions were mixed at a component weight ratio of 60/40 to obtain a chitosan/PCL solution, and the mixed solution was used immediately to avoid degradation of PCL. To prepare the polyvinylidene fluoride (PVDF) solution, polyvinylidene fluoride tetrafluoroethylene (PVDF−TFE, MW 180 000 Da, Arkema Corporation, King of Prussia, PA) and PVDF (MW 180 000 Da, Arkema Corporation, King of Prussia, PA) were mixed at a weight ratio of 70/30. The mixture was dissolved in a solvent with a dimethyl formamide (DMF)/acetone weight ratio of 60/40 to create a final polymer concentration of 25 wt %. To prepare the titanium tetraisopropoxide solution, 1 g of titanium tetraisopropoxide (Aldrich), 1 mL of 2-propanol, and 1 mL of acetic acid were mixed with a solution containing 0.15 g of poly(vinyl pyrrolidone) (PVP, MW 29 000 Da, Aldrich) and 3 mL of 2-propanol, and the mixture was stirred for 1 h.

Electrospinning Parameters. Electrospinning of PCL solution was performed with the following conditions: spinneret−collector distance of 15 cm, spinneret angle of 15° (depression angle), and a 15 kV dc applied voltage. The chitosan/PCL nanofibers were prepared with the following conditions: spinneret−collector distance of 12 cm, spinneret angle of 12°, and a 12 kV applied voltage. The PVDF fiber samples were prepared with the following conditions: spinneret−collector distance of 15 cm, spinneret angle of 17°, and a 10 kV applied voltage. The TiO_2/PVP nanofiber samples were prepared with the following conditions: spinneret−collector distance of 8 cm, spinneret angle of 12°, and a 12 kV applied voltage.

Fibrous Construct Characterizations. The fibrous samples were retrieved from the pin electrode gap (collector). For morphology analysis, the PCL, chitosan/PCL, and PVDF fibrous samples were sputter-coated with Au/Gd for 50 s at 18 mA. The TiO_2/PVP composite cylinders and the calcinated cylinders were not sputter coated. The samples were imaged with a scanning electron microscope (SEM, JEOL JSM 7000F) at an operating voltage of 10 kV. TiO_2/PVP composite scafffolds were calcined at 500 °C for 3 h to remove PVP and produce TiO_2 fibers. Energy-dispersive X-ray spectroscopy (EDS) was used for elemental analysis of calcined TiO_2 samples. The X-ray diffraction (XRD) patterns of calcined TiO_2 samples were obtained using a Philips PW-1710 diffractometer (Cu Kα radiation) at a scanning rate of 0.02°/s over a 2θ range of 20° to 80°, operated at 40 kV and 40 mA. For PCL and chitosan/PCL samples, the 2θ range was 5° to 50°, operated at 40 kV and 20 mA

To quantify the degree of fiber alignment of nanofibrous cylinders, SEM images were taken at three random locations of a cylinder sample and the orientation of 50 fibers on each image was measured using ImageJ v1.38 (NIH, Bethesda, MD, USA). A reference line was drawn along the central orientation, and the fiber orientation was evaluated by measuring the angle between a line drawn along the fiber and a line parallel to the central line.

The porosity of the nanofibrous cylinders were evaluated using the formula:[26]

$$\text{apparent density of nanofibrous scaffold (g/cc)} = \frac{\text{mass of the nanofibrous scaffold (g)}}{\text{volume of the nanofibrous scaffold (cc)}}$$

$$\text{porosity of the scaffold} = \left(1 - \frac{\text{apparent density of the scaffold}}{\text{bulk density of scaffold material}}\right)$$

The volume of the nanofibrous scaffolds was determined by the scaffold thickness (cm) × area (cm^2). The bulk material was produced by pouring the polymer solution in a defined shaped mold and then solidifying in a vacuum drying oven. The bulk density was then calculated from its mass and volume. The dimensions of nanofiber cylinders were measured with a micrometer (Mitutoyo, Japan) and a caliper (Mitutoyu, Japan).

Fourier transmission infrared (FTIR) spectroscopy was performed on chitosan, PCL, and chitosan/PCL samples using a Nicolet 5DX spectrometer at 4 cm^{-1} resolution. All samples were pulverized and mixed with potassium bromide (KBr). The resultant suspensions were pressed to transparent pellets and examined in absorbance mode within the range of 4000−400 cm^{-1}.

Thermal properties of chitosan/PCL and PCL nanofibrous cylinders were studied by differential scanning calorimetry (DSC) in a Q100 calorimeter with a refrigerated cooling system (TA Instruments) under a nitrogen atmosphere at a heating rate 5 °C/min in the range of 35−100 °C.

In Vitro Cell Study. C2C12 muscle cells (mouse myoblast cell line) were obtained from American Type Culture Collection (Arlington, VA). The culture medium was Dulbecco's modified Eagle's medium (DMEM, Invitrogen, Carlsbad, CA) supplemented with 10% fetal bovine serum (FBS, Invitrogen) and 1% penicillin−streptomycin (Invitrogen). Prior to cell seeding, nanofibrous chitosan/PCL scaffolds were sterilized, placed in 24-well culture plates, and incubated overnight in phosphate buffer saline (PBS, Invitrogen) at 4 °C. Scaffolds were cultured with 100 000 muscle cells per sample and analyzed after 10 days.

The cell morphology on the nanofibrous construct was examined by SEM. The samples were rinsed in PBS and fixed in Karnovsky's fixative overnight. After fixing, samples were briefly rinsed in DI water and dehydrated by sequential incubation in 50, 75, and 100% ethanol for 15 min each at room temperature. The samples were dried with a critical point dryer (Denton DCP-1, Cherry Hill, NJ), sputter-coated with Au/Pd for 60 s at 18 mA, and imaged with SEM.

For immunofluorescent staining, samples were rinsed in PBS and fixed with 4 v % paraformaldehyde in PBS overnight at 4 °C. The samples were then washed in ice-cold PBS and permeabilized with 0.025% Triton X-100 (Aldrich) in PBS for 15 min. The samples were incubated in 10% rabbit serum (Abcam, Cambridge, MA) in PBS for 45 min to block nonspecific protein binding and in mouse myosin heavy chain (MHC, MY-32, Abcam) antibody at a 1:400 dilution in PBS with 0.025% Triton X-100 overnight at 4 °C. The samples were then incubated in a 1:400 dilution of Texas Red conjugated mouse secondary antibody (Abcam) in PBS for 45 min. For actin staining, fluorescein isothiocyanate (FITC)−phalloidin (Invitrogen) was added to the secondary antibody solution at a 1:50 dilution and the samples were incubated for 20 min. All incubation steps, except the overnight incubation, were performed at room temperature, and the samples were rinsed three times in PBS after each step. The samples were rinsed in PBS and mounted to a coverslip with Prolong Gold Antifade reagent with 4′,6-diamidino-2-phenylindole (DAPI, Invitrogen). The samples were cured overnight and imaged with a confocal fluorescent microscope (Zeiss Meta Confocal, Germany).

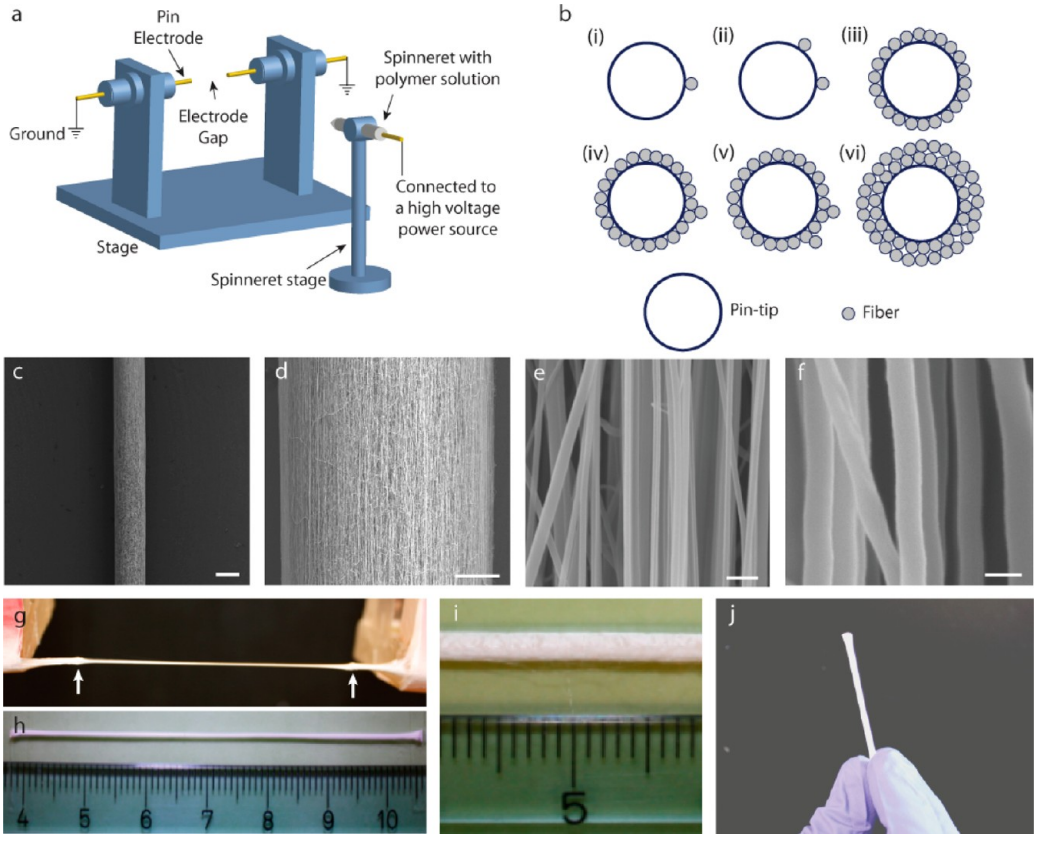

Figure 1. Novel electrospinning system for fabrication of aligned nanofibrous cylinders. (a) Schematic of the electrospinning system consisting of two grounded conductive pin electrodes separated by an electrode gap. (b) Schematic representation of a cylindrical nanofibrous structure produced by layer-by-layer fiber deposition. (c–f) SEM images of the PCL fibrous construct at different magnifications, where the scale bars indicate 200 μm, 50 μm, 2 μm, and 200 nm from c to f, respectively. (g) Photograph of an aligned nanofibrous cylinder formed between the pin electrodes (white arrows) after electrospinning a 12 wt % PCL solution for 30 min at a spinneret–electrode distance of 12 cm. (h) Photograph of a ~7 cm long PCL fibrous construct. (i) Photograph of a PCL fibrous cylinder with a diameter of ~2 mm. (j) A typical standalone PCL nanofibrous cylinder collected from the pin electrodes.

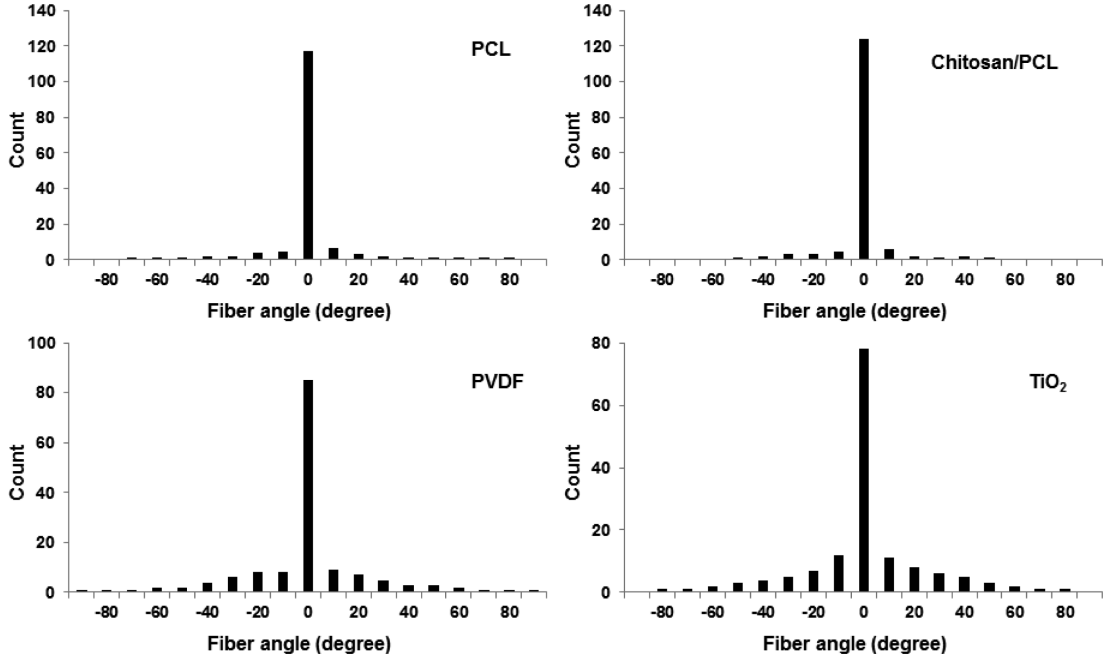

Figure 2. Fiber orientation distribution in nanofibrous cylinders made from different materials as quantified by the ImageJ software. A total of 150 fibers were measured at 3 randomly selected places for each sample.

dx.doi.org/10.1021/am301803b | ACS Appl. Mater. Interfaces 2012, 4, 4817–4824

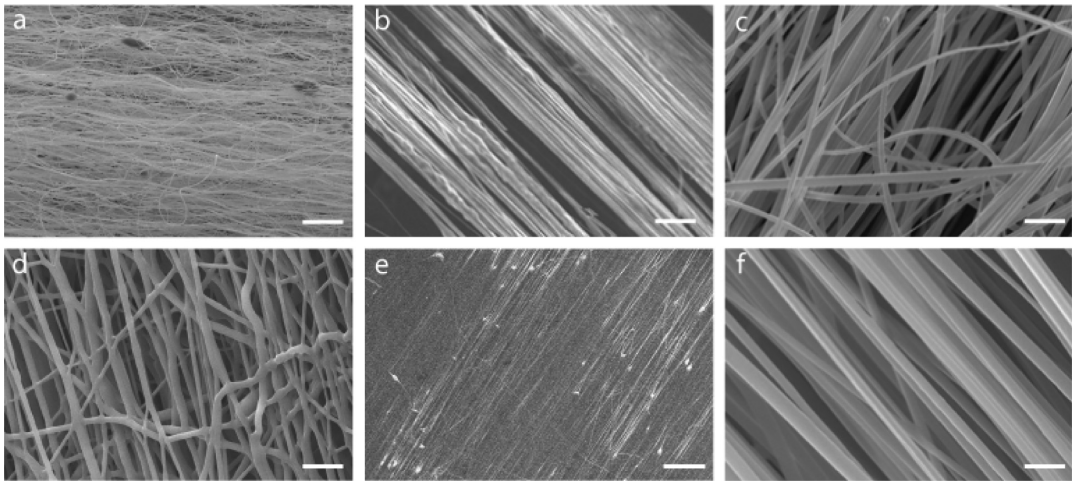

Figure 3. SEM images of PCL fiber morphology as a function of electrospinning parameters. (a) Less aligned fibers produced at an electrode gap width of <1 cm. Scale bar = 2 μm. (b) Aligned fibers with beads produced at a spinneret−electrode distance of >3 cm. Scale bar = 1 μm. (c) Reduced fiber alignment at high voltage (>17 kV). Scale bar = 1 μm. (d) Mesh-like fiber membrane formed due to high viscosity. Scale bar = 750 nm. (e) Entangled fibers with beads (white spots) due to high spinneret angle (>15°; feed rate > 1.8 mL/h). Scale bar = 3 μm. (f) Aligned fibers spun with optimal parameters. Scale bar = 300 nm.

RESULTS AND DISCUSSION

The electrospinning system developed for production of highly aligned nanofibrous cylinders is illustrated in Figure 1a. A nonconductive stage supports two grounded pin electrodes which are uniaxially aligned and separated by an adjustable gap that serves as the fiber collector. A spinneret filled with material solution is supported by a second stage, placed a distance from the collector, and oriented perpendicular to the electrode axis. The material solution is powered by a high-voltage power supply via a platinum wire and dispensed by electrostatic and gravitational forces. The distance between the spinneret and electrode axis is adjusted by moving the spinneret-holding stage. During electrospinning, the positively charged solution jet is driven toward the grounded electrodes. Near the electrode gap, the electrostatic field pulls the leading tip of the fiber to one electrode and the trailing end to the other, aligning the deposited fiber along the electrode axis across the gap. Figure 1b(i) shows an illustration of the cross-sectional view of the first fiber deposited on an electrode. Because of the poor conductivity of the polymer, the deposited fiber retains a positive charge and the resultant electrostatic force repeals incoming fibers. Thus, a second fiber would attach to the electrode surface area not covered by the fiber (Figure 1b(ii)). This process continues until the electrode surface is covered by a single layer of fibers (Figure 1b(iii)), wherein the surface of the electrode is equipotential. A second layer of fibers is similarly deposited on the first fiber layer (Figure 1b(iv−vi)). An aligned fibrous cylinder is thus created by layer-by-layer deposition.

A 12 wt % PCL solution was first used to demonstrate the electrospinning system. SEM analysis shows that a PCL fibrous cylinder of ∼200 μm in diameter was produced after 30 min of electrospinning (Figure 1c,d). A high degree of fiber alignment and a fiber diameter of 50−200 nm were observed at high magnification (Figures 1e,f), and the standalone cylinder was ∼4 cm in length (Figure 1g). The cylinder can be produced up to ∼7 cm in length (Figure 1h). The degree of fiber alignment, quantified by the ImageJ software, further confirmed that the majority of PCL fibers were aligned uniaxially (Figure 2, top, left panel). The fibers in the cylinder were mostly distributed discretely providing a large collective surface area which is highly desirable in sensors, capacitance systems, and other detection devices.[27,28] Fibrous cylinders with larger diameters can be produced by prolonged electrospinning, and PCL nanofibrous cylinders with a diameter of ∼2 mm have been produced (Figure 1i). The measured porosity of the cylinder was 84%. Notably, the electrospun cylindrical construct can be easily removed from the collector and serve as a standalone construct without support of a substrate (Figure 1j).

As with all the electrospinning systems, the material solution characteristics and electrospinning parameters dictate the fiber formation and degree of fiber alignment.[29] In our system setup, the influence of major operating parameters on the fiber formation and properties such as fiber diameter, morphology, and cylinder structure was investigated, including the solution viscosity, applied voltage, distance between two pin electrodes, distance between the spinneret and fiber collector, and polymer feed rate using PCL solution.

The distance between the two electrode tips can greatly affect the fiber diameter, alignment, and structural integrity of the produced construct. If the gap is too small (<1 cm), fibers accumulate fast but are not well aligned or uniform and have relatively large fiber diameter, presumably due to the limited space that prevents the polymer jet from fully stretching (Figure 3a). With increasing electrode gap width, the degree of fiber alignment increases and the fiber diameter decreases. However, there is a critical gap width, beyond which most fibers are not deposited across the gap but directly on pin electrodes. For PCL solution, the minimum width to obtain fiber alignment is ∼1 cm and maximum width is ∼7 cm.

Similarly, the distance between the spinneret and electrode axis (collector) affects the fiber formation and the cylindrical structure. If this distance is too small (<3 cm), the polymer solution drawn out of the spinneret by gravitational force falls to the stage of the electrospinning system because the distance is insufficient for solvent to evaporate and form fibers. In addition, a higher electrostatic force at the smaller distance also breaks up the solution jet to form droplets. The solution jet undergoes the following changes with gradually increasing spinneret−electrode axis distance: aligned fibers with discrete

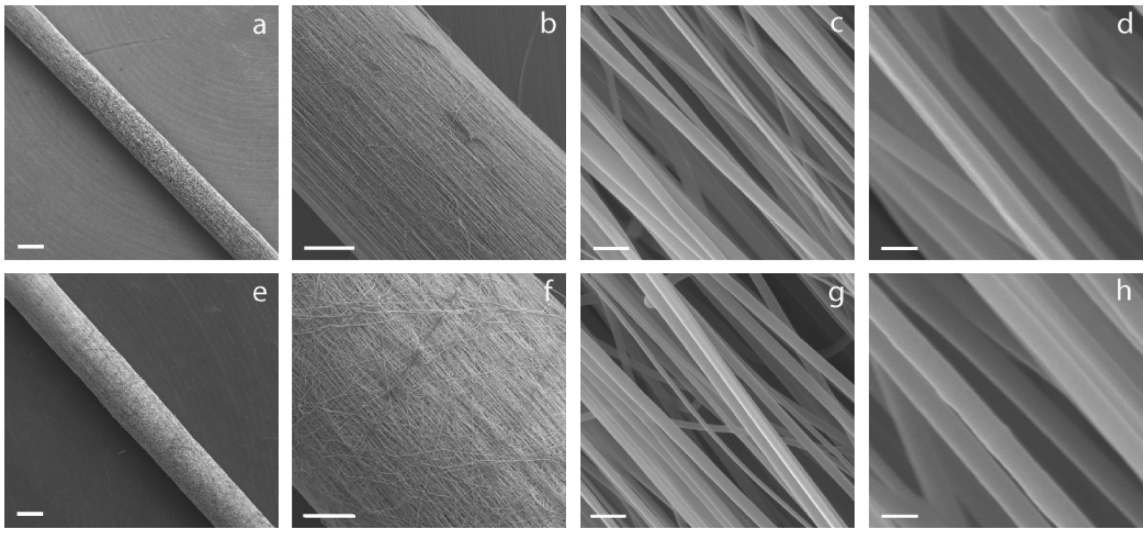

Figure 4. SEM images of aligned nanofibrous cylindrical constructs. (a–d) A chitosan/PCL fibrous construct, where the scale bars represent 200 μm, 50 μm, 500 nm, and 200 nm, respectively. (e–h) A PVDF fibrous construct, where the scale bars represent 200 μm, 50 μm, 1 μm, and 400 nm, respectively.

beads in the structure (Figure 3b), aligned fibers, and aligned fibers with smaller diameters (Figure 1c–f). A further increase in this distance causes polymer fibers to randomly deposit on the stage rather than across the gap, presumably because the strength of the oriented electric field near the electrodes is insufficient to pull fibers to the collector. The critical distance between the spinneret and collector for the 12 wt % PCL solution at a voltage of 12 kV was ~15 cm.

The applied electrical voltage also plays a role in the fiber deposition. At a low voltage (e.g., <7 kV), the electrostatic force is unable to overcome the surface tension of the polymer solution jet. As a result, the polymer solution falls to the stage as droplets. At a higher voltage (~12–17 kV), the charged solution overcomes the surface tension and the solution jet is elongated to form a fiber.[18] At an even higher voltage (~17–20 kV), fibers with small diameters are formed due to solution jet thinning (Figure 3c). This simultaneous deposition of multiple fibers can reduce the degree of fiber alignment, as most of the fibers do not sufficiently stretch to span across the two electrodes. Thus, for each polymer solution and concentration, the best fiber quality was obtained in a defined voltage range (e.g., 12–15 kV for 12 wt % PCL with a collector–spinneret distance of 15 cm).

The viscosity of a polymer solution is normally proportionally related to the polymer concentration and is critical to the production and quality of aligned fibers by electrospinning. At a relatively low viscosity, breakup of the solution jet occurs due to the lower cohesion force in the solution, and solution droplets are created by electrospraying.[30] If the viscosity is too high, fibers tend to coalesce because they are not fully dried upon deposition, and consequently, a mesh-like fiber membrane is created (Figure 3d). Thus, for each polymer and solvent, there is an optimal viscosity (or polymer concentration) at which thin, discrete fibers can be produced. For the PCL system, the 12 wt % solution yielded the best quality of nanofibers.

In our electrospinning system, the angle of the spinneret elevation determines the solution feed rate. If the feed rate is too low (e.g., feed rate < 0.7 mL/h at the angle < 5°), the fiber production is slow. Conversely, a high feed rate (e.g., feed rate > 1.8 mL/h at the angle > 15°) may result in fibers with large diameters, fiber entanglements, and embedded beads (Figure 3e). In addition, part of the solution that comes out of the spinneret will fall to the stage. For the 12 wt % PCL solution, a 15° spinneret angle (feed rate = 1.8 mL/h) was optimal for producing nanofibrous cylinders with no beads and minimal entanglements. By applying the optimal parameters including a gap distance of ~2 cm, a distance of ~15 cm between the collector and spinneret, an applied voltage of ~15 kV, and the spinneret angle of 15°, aligned nanofibers with diameters of 50–200 nm were obtained by spinning a 12 wt % PCL solution (Figure 3f).

In addition to PCL, chitosan/PCL and PVDF polymer solutions were electrospun to demonstrate the broader applicability of our system. Following the similar procedure discussed above, chitosan/PCL fibrous cylinders were fabricated with a diameter of 200 μm after 20 min of electrospinning (Figures 4a,b). The fibers were mostly aligned (Figure 4c) with diameters of 100–200 nm (Figure 4d). The porosity of the cylindrical scaffold was 77%. For PVDF, a 400 μm diameter cylinder with aligned fibers was obtained after 20 min of electrospinning (Figure 4e–g). The fiber diameters ranged from 350 to 500 nm (Figure 4h). The porosity of the PVDF construct was 83%. Figure 2 shows the distribution of fiber orientation for chitosan/PCL and PVDF fibrous cylinders (top, right panel and bottom, left panel, respectively), indicating that both fibrous constructs have highly aligned fibers.

To determine the molecular interaction between PCL and chitosan in chitosan/PCL nanofibers, FTIR was performed on PCL, chitosan/PCL, and chitosan samples (Figure 5a). The characteristic bands at 2942, 1725, and 1245 cm^{-1} correspond to the ester group of PCL whereas bands at 1648 and 1576 cm^{-1} correspond to amide-I and amide-II of chitosan.[31] There are no significant frequency shifts of charactreristic functional groups in chitsoan-PCL nanofibers compared to chitosan and PCL samples. This indicates that there was no chemical bonding between PCL and chitosan components in the blend nanofibers.

X-ray diffraction patterns of chitosan/PCL and PCL nanofibers (Figure 5b) show that there was significant

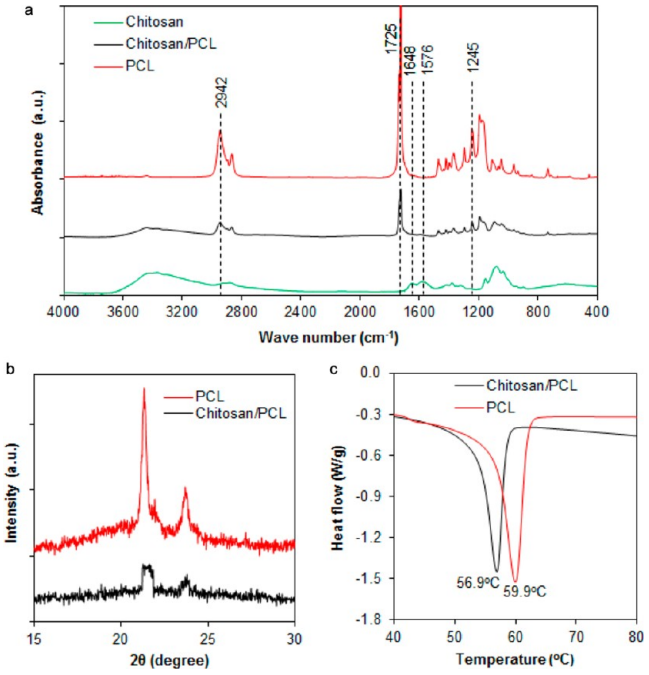

Figure 5. Chemical and physical characteristics of chitosan/PCL nanofibers. (a) FTIR spectra of chitosan film, chitosan/PCL, and PCL nanofibers with highlighted characteristic bands. (b) XRD patterns of PCL and chitosan/PCL nanofibers. (c) DSC thermograms of PCL and chitosan/PCL nanofibers.

weakening of characteristic PCL peaks at 21.5° and 23.6°[21] due to the addition of chitosan. This indicates that the addition of chitosan reduced the crystallinty of PCL, signifying good miscibility of component materials in the chitosan/PCL blend.[32]

The DSC thermograms of chitosan/PCL nanofibers indicate that the melting temperature of chitosan/PCL is 56.9 °C, compared to the melting temperature of pure PCL which is 59.9 °C (Figure 5c). This reduction in melting temperature and the absence of additional peaks further confirm the good miscibility of the chitosan and PCL.

The system was further used to produce a nanofibrous cylinder of a metal oxide, TiO_2 (titania). The titania fibrous cylinder was produced from a titanium tetraisopropoxide/PVP solution in 2-propanol and acetic acid.

Titanium tetraisopropoxide hydrolyzes in air to create amorphous TiO_2. The produced TiO_2/PVP composite nanofibrous cylinder had a diameter of ~225 μm (Figures 6a,b) after 30 min of electrospinning and fiber diameters of 100−300 nm (Figure 6c). The surface of the TiO_2/PVP composite nanofiber appeared smooth (Figure 6d), indicating the uniform dispersion of TiO_2 in the PVP polymer matrix. After calcination of the composite sample at 500 °C for 3 h, the TiO_2 cylinder diameter was reduced to ~175 μm (Figure 6e−g), as a result of the removal of PVP and crystallization of titania at high temperature. Figure 2 shows that TiO_2 fibers in the cylinder were highly aligned (bottom, right panel). The SEM image of a single TiO_2 nanofiber at high resolution (Figure 6h) reveals that the solid fiber is composed of TiO_2 nanoparticles of ~5−10 nm in diameter (inset). The porosity of the TiO_2 scaffold was determined to be 92%. EDS of the calcined sample showed the characteristic peaks of Ti element (4.5 and 4.9 KeV) and of oxygen element (0.6 KeV)[33] and confirmed the presence of only titanium and oxygen in the fibrous structure (Figure 6i). All the diffraction peaks can be indexed to anatase phase of titania (JCPDS files no. 21-1272) based on XRD analysis (Figure 6j).

As a model biomedical application, we investigated applicability of growing myotubes from muscle cells on aligned chitosan/PCL nanofibrous cylinders as scaffolds for skeletal muscle engineering. The structure of native muscle is composed of highly oriented multinucleated myofibers formed from the fusion of muscle cells. Muscle growth or regeneration involves the myotube formation and alignment. It is well-known that the structure and organization of muscular fibers dictate tissue function, and the muscle cell alignment that permits organized myotube formation is critical to the musculoskeletal myogenesis.[34] Chitosan/PCL nanofibrous scaffolds have previously demonstrated enhanced myogenesis and muscle cell alignment and partial myotube formation.[14] In this study, we cultured myoblast cells on chitosan/PCL aligned nanofibrous cylinders of 1 mm diameter and 1 cm long for 10 days without using differentiation-inducing media to investigate their attachment, growth, and myotube formation. After culture, the samples were recovered, fixed, and imaged by SEM and confocal fluorescence microscopy. The SEM images showed that a large number of myotubes formed and elongated along the orientation of aligned nanofibers (shown by arrow; Figure 7a,b, the first column). Figure 7a at a low magnification and Figure 7b at a high magnification showed the fluorescence images of muscle cells immuno-stained with antibodies against actin and myosin heavy chain (MHC) along nanofibrous cylinders. The expression of actin (a muscle component) and MHC (a protein required for myotube formation) by muscle cells are the indicators of muscle cell proliferation and differentiation, respectively. The myotubes were seen parallel to each other and elongated along the orientation of fiber alignment. It was noted that the aligned myoblast cells were fused to form aligned myotubes (Figure 7, the fourth column) without any external reagents such as growth factors or reduced conditions that are typically required for in vitro culture. This indicates that the uniaxially aligned fibers in the scaffold indeed promoted the cell migration, elongation, and maturation along the orientation of fiber alignment to form a natural tissue-mimicking muscle structure and organization. Significantly, densely populated myotubes were formed on the nanofibrous cylindrical scaffold without support of a substrate or other material, which can serve as a standalone tissue construct for subsequent implantation.

CONCLUSIONS

We have presented a simple approach to fabricate 3D aligned nanofibrous cylindrical constructs using electrospinning. This electrospinning approach fabricates nanofibrous cylinders by depositing aligned fibers in a layer-by-layer fashion across the gap of a pair of conductive electrodes. The diameter and length of the cylinder are defined by the duration of electrospinning and the width of the electrode gap, respectively. The diameter of the nanofibers and degree of fiber alignment depend strongly on the solution properties, solution feed rate, the distance between the spinneret and collector, the electrode gap width, and the applied voltage. The potential applicability of this technique for diverse material systems was demonstrated with several widely used materials, including two synthetic polymers, a natural/synthetic polyblend, and a ceramic material. In demonstrating aligned nanofibrous cylinders as scaffolds for tissue engineering, myoblast cells cultured on chitosan/PCL

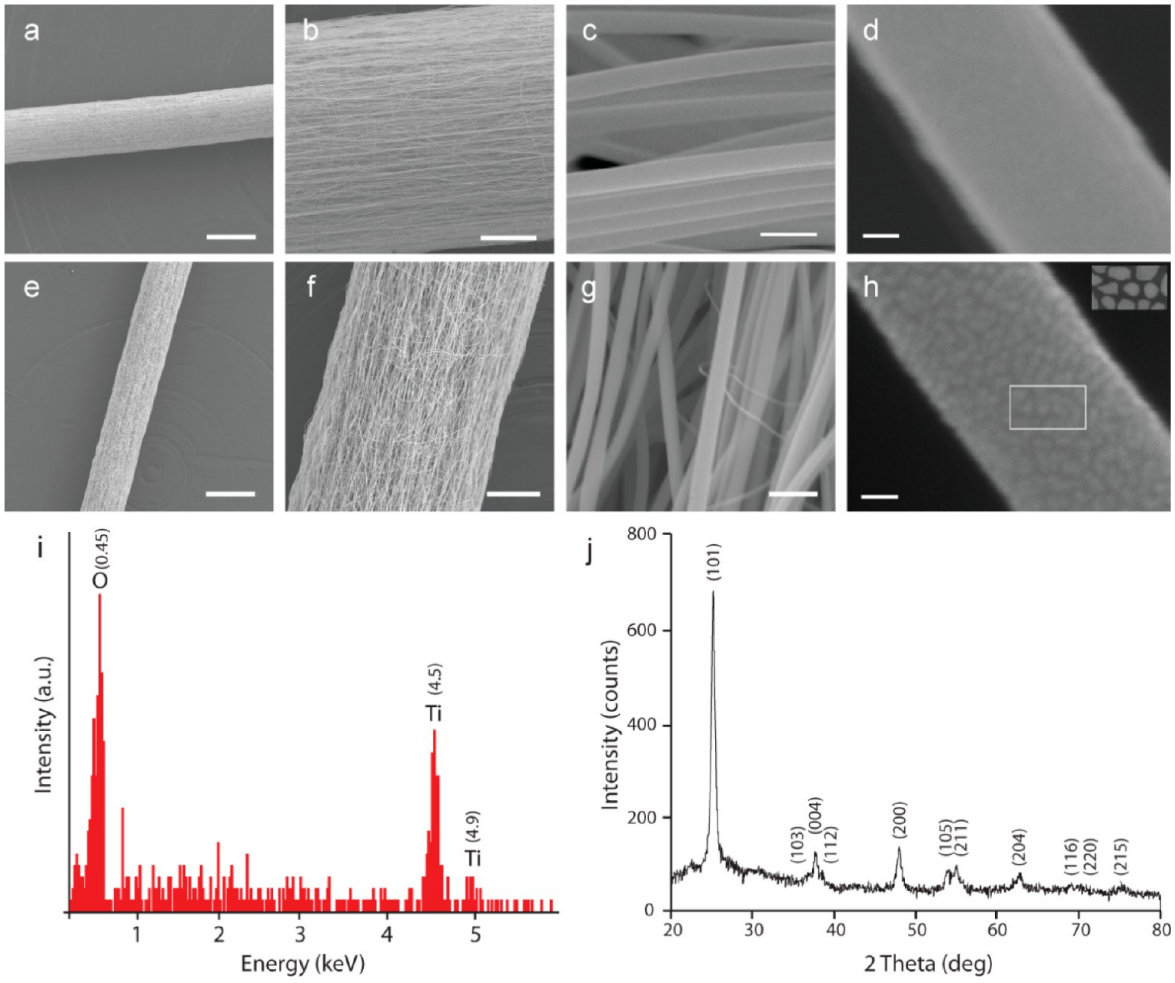

Figure 6. Inorganic nanofibrous cylindrical samples and their characterizations. (a–d) SEM images of a TiO_2/PVP aligned nanofibrous cylinder, where the scale bars indicate 200 μm, 50 μm, 1 μm, and 20 nm, respectively. (e–h) SEM images of aligned TiO_2 nanofibrous cylinder produced by calcination of the TiO_2/PVP sample shown in panels a–d at 500 °C for 3 h to remove PVP, where the scale bars indicate 200 μm, 50 μm, 1 μm, and 20 nm, respectively. The inset in (h) is the contrast enhanced image of the area marked with a white frame. (i) EDS of the TiO_2 sample showing Ti and O peaks. (j) XRD pattern of the TiO_2 sample.

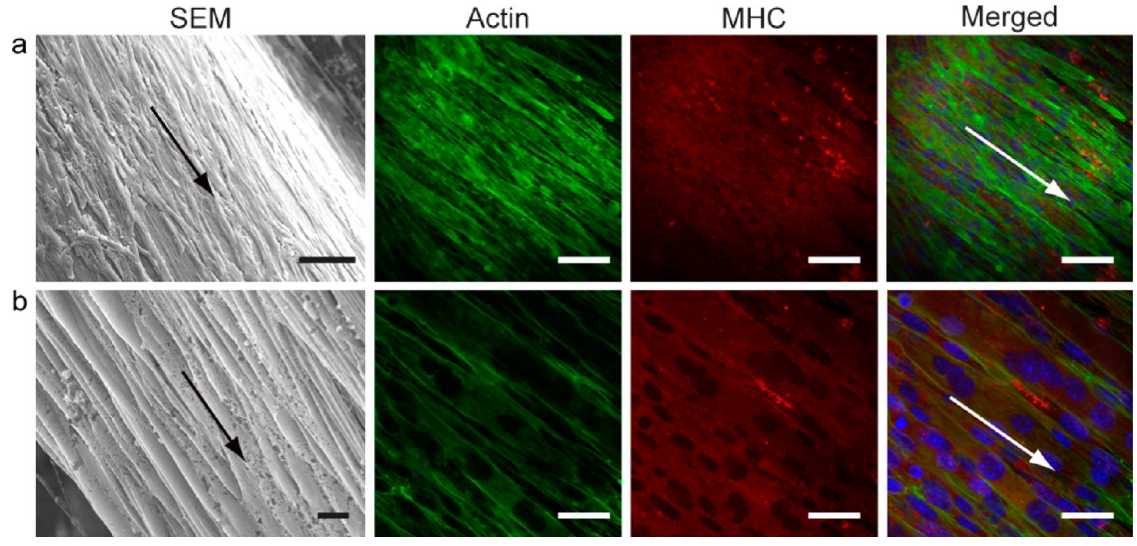

Figure 7. SEM and immunostained images of myotubes grown on chitosan/PCL nanofibrous cylinders after 10 days of cell culture. Fibrous cylinders were immuno-stained for actin (green) and MHC (red) expressed by C2C12 muscle cells in myotubes with DAPI staining of nuclei (blue). (a) Images at low magnification. Scale bars indicate 100, 60, 60, and 60 μm, respectively. (b) Images at high magnification. Scale bars indicate 10, 20, 20, and 20 μm, respectively.

nanofibrous cylindrical scaffolds formed aligned, densely populated myotubes required for skeletal muscle tissue regeneration. The aligned nanofibrous cylinders fabricated with this technique can be used without a substrate support for diverse applications.

AUTHOR INFORMATION

Corresponding Author

*E-mail: mzhang@u.washington.edu.

Notes

The authors declare no competing financial interest.

ACKNOWLEDGMENTS

This work is supported in part by the Kyocera Professor Endowment. A.C. would like to acknowledge the support by the Bank of America Endowed Minority Fellowship.

REFERENCES

(1) Beachley, V.; Katsanevakis, E.; Zhang, N.; Wen, X. In *Biomedical Applications of Polymeric Nanofibers*; Jayakumar, R., Nair, S. V., Eds.; Springer-Verlag: Berlin Heidelberg, 2012; Vol. *246*, pp 171.
(2) Du, F.; Wang, H.; Zhao, W.; Li, D.; Kong, D.; Yang, J.; Zhang, Y. *Biomaterials* **2012**, *33*, 762−770.
(3) Holzwarth, J. M.; Ma, P. X. *Biomaterials* **2011**, *32*, 9622−9629.
(4) Sur, S.; Pashuck, E. T.; Guler, M. O.; Ito, M.; Stupp, S. I.; Launey, T. *Biomaterials* **2012**, *33*, 545−555.
(5) Tamaru, S.-I.; Ikeda, M.; Shimidzu, Y.; Matsumoto, S.; Takeuchi, S.; Hamachi, I. *Nat. Commun.* **2010**, *1*, 20.
(6) Huang, Z.; Lee, H.; Lee, E.; Kang, S.-K.; Nam, J.-M.; Lee, M. *Nat. Commun.* **2011**, *2*, 459.
(7) Wu, H.; Hu, L.; Rowell, M. W.; Kong, D.; Cha, J. J.; McDonough, J. R.; Zhu, J.; Yang, Y.; McGehee, M. D.; Cui, Y. *Nano Lett.* **2010**, *10*, 4242−4248.
(8) Wang, W.; Lu, X.; Li, Z.; Lei, J.; Liu, X.; Wang, Z.; Zhang, H.; Wang, C. *Adv. Mater.* **2011**, *23*, 5109−5112.
(9) Lee, S. W.; Lee, H. J.; Choi, J. H.; Koh, W. G.; Myoung, J. M.; Hur, J. H.; Park, J. J.; Cho, J. H.; Jeong, U. *Nano Lett.* **2010**, *10*, 347−351.
(10) Chen, X.; Xu, S.; Yao, N.; Shi, Y. *Nano Lett.* **2010**, *10*, 2133−2137.
(11) Mitchell, R. R.; Gallant, B. M.; Thompson, C. V.; Shao-Horn, Y. *Energy Environ. Sci.* **2011**, *4*, 2952−2958.
(12) Tamura, T.; Kawakami, H. *Nano Lett.* **2010**, *10*, 1324−1328.
(13) Zhi, M.; Mariani, N.; Gemmen, R.; Gerdes, K.; Wu, N. *Energy Environ. Sci.* **2011**, *4*, 417−420.
(14) Cooper, A.; Jana, S.; Bhattarai, N.; Zhang, M. Q. *J. Mater. Chem.* **2010**, *20*, 8904−8911.
(15) Jin, G.-Z.; Kim, M.; Shin, U. S.; Kim, H.-W. *Neurosci. Lett.* **2011**, *501*, 10−14.
(16) Tse, K. Y.; Zhang, L. Z.; Baker, S. E.; Nichols, B. M.; West, R.; Hamers, R. J. *Chem. Mater.* **2007**, *19*, 5734−5741.
(17) Luo, C. J.; Stoyanov, S. D.; Stride, E.; Pelan, E.; Edirisinghe, M. *Chem. Soc. Rev.* **2012**, *41*, 4708−4735.
(18) Bhardwaj, N.; Kundu, S. C. *Biotechnol. Adv.* **2010**, *28*, 325−347.
(19) Cavaliere, S.; Subianto, S.; Savych, I.; Jones, D. J.; Roziere, J. *Energy Environ. Sci.* **2011**, *4*, 4761−4785.
(20) Badrossamay, M. R.; McIlwee, H. A.; Goss, J. A.; Parker, K. K. *Nano Lett.* **2010**, *10*, 2257−2261.
(21) Bhattarai, N.; Li, Z.; Gunn, J.; Leung, M.; Cooper, A.; Edmondson, D.; Veiseh, O.; Chen, M.-H.; Zhang, Y.; Ellenbogen, R. G.; Zhang, M. *Adv. Mater.* **2009**, *21*, 2792−2797.
(22) Wang, C. Y.; Zhang, K. H.; Fan, C. Y.; Mo, X. M.; Ruan, H. J.; Li, F. F. *Acta Biomater.* **2011**, *7*, 634−643.
(23) Kean, T.; Thanou, M. *Adv. Drug Delivery Rev.* **2010**, *62*, 3−11.
(24) Rathod, V. T.; Mahapatra, D. R.; Jain, A.; Gayathri, A. *Sens. Actuators, A* **2010**, *163*, 164−171.
(25) Krishnamoorthy, T.; Thavasi, V.; Subodh, M. G.; Ramakrishna, S. *Energy Environ. Sci.* **2011**, *4*, 2807−2812.
(26) Zhang, K.; Qian, Y.; Wang, H.; Fan, L.; Huang, C.; Yin, A.; Mo, X. *J. Biomed. Mater. Res., Part A* **2010**, *95A*, 870−881.
(27) Liu, J. W.; Essner, J.; Li, J. *Chem. Mater.* **2010**, *22*, 5022−5030.
(28) Moon, J.; Park, J. A.; Lee, S. J.; Zyung, T.; Kim, I. D. *Sens. Actuators, B* **2010**, *149*, 301−305.
(29) Park, S. H.; Yang, D.-Y. *J. Appl. Polym. Sci.* **2011**, *120*, 1800−1807.
(30) Rutledge, G. C.; Fridrikh, S. V. *Adv. Drug Delivery Rev.* **2007**, *59*, 1384−1391.
(31) Neves, S. C.; Teixeira, L. S. M.; Moroni, L.; Reis, R. L.; Van Blitterswijk, C. A.; Alves, N. M.; Karperien, M.; Mano, J. F. *Biomaterials* **2011**, *32*, 1068−1079.
(32) Bhattarai, N.; Li, Z.; Gunn, J.; Leung, M.; Cooper, A.; Edmondson, D.; Veiseh, O.; Chen, M.; Zhang, Y.; Ellenbogen, R.; Zhang, M. *Adv. Mater.* **2009**, *21*, 2792−2797.
(33) Wu, N.; Xia, X.; Wei, Q. F.; Huang, F. L. *Fibres Text. East. Eur.* **2010**, *18*, 21−23.
(34) Choi, J. S.; Lee, S. J.; Christ, G. J.; Atala, A.; Yoo, J. J. *Biomaterials* **2008**, *29*, 2899−2906.